



Biosynthesis of Ag and Fe nanoparticles using *Erodium cicutarium*; study, optimization, and modeling of the antibacterial properties using response surface methodology

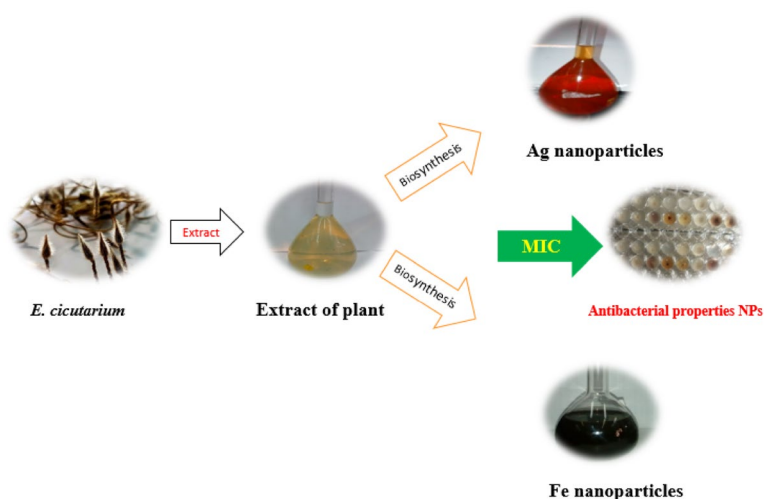
Nahid Maghsoudy¹ · Parviz Aberoomand Azar¹ · Mohammad Saber Tehrani¹ · Syed Waqif Husain¹ · Kambiz Larijani¹

Received: 17 March 2019 / Accepted: 26 June 2019 / Published online: 10 August 2019
© The Author(s) 2019

Abstract

The present study deals with the preparation of silver (Ag) and iron (Fe) nanoparticles, extracted from AgNO₃ and FeSO₄·7H₂O solutions, respectively. For this, the aqueous extract of *Erodium cicutarium* was used. The Ag and Fe nanoparticles were characterized by several techniques such as X-ray diffraction (XRD), field emission scanning electron microscope (FE-SEM), energy dispersive X-ray (EDX) spectrometer, UV–visible, and Fourier transform infrared (FTIR) spectroscopy. FE-SEM images showed that the Ag and Fe particles had nearly spherical morphology with diameters less than 100 nm. Low amounts of impurity and different chemicals in the prepared nanoparticles were confirmed by EDX spectrometers. Furthermore, different functional groups in the nanoparticles were indicated using FTIR spectrum. Antibacterial activity of the Ag and Fe nanoparticles was evaluated by minimum inhibitory concentration (MIC) for *E. coli* and *S. aureus* bacteria. Two parameters such as the concentration of Ag and Fe nanoparticles (X_1) and pH (X_2) were modeled by the use of the response surface methodology (RSM). These experiments were carried out as a central composite design (CCD) consisting of 13 experiments. The results showed that the concentration of Ag and Fe nanoparticles had a better effect on antibacterial activity. Under optimal conditions—with concentrations of Ag and Fe nanoparticles at 399.53 and 397.38 (μg/mL) and pH values of 8.20 and 8.39, respectively—the bacterial growth inhibition halo was found to have the highest diameter.

Graphic abstract



Keywords Ag and Fe nanoparticles · *Erodium cicutarium* · Antibacterial activity · RSM · CCD

✉ Parviz Aberoomand Azar
parvzaberoomand@gmail.com

Extended author information available on the last page of the article



Introduction

Nowadays, special attention is being given to green synthesis of metal nanoparticles [1]. A number of approaches including thermal decomposition, microwave-assisted process, and green chemistry are available for the synthesis of many nanoparticles (especially the silver ones) [2]. The inorganic materials, especially metal nanoparticles, are widely biosynthesized by biological materials such as microorganisms and plants [3, 4]. Metal nanoparticles perform antimicrobial activity and their potential applications as antibacterial agent in food packaging has been reported [5]. The synthesis of gold and silver nanoparticles was first reported by Gardea-Torresdey et al. [6, 7] done using living alfalfa plants. Recently, the synthesis of the following were reported: gold nano-triangles and silver nanoparticles (using *Aloe vera* plant extracts) [8], silver and gold nanoparticles (by *Cinnamomum camphora* leaf) [9], silver nanoparticles (using aqueous seed extracts of *Macrotyloma uniflorum* [1], *Cocos nucifera* coir [10], *Solanum trilobatum*, *Syzygium cumini*, *Centella asiatica*, *Citrus sinensis* powders, and from an aqueous mixture of *Ficus carica* leaf extract), and AgNO_3 solution [11]. Essential oil was used as excellent food flavoring, pharmaceutical, and non-traditional medicine compounds. Plant-derived essential oils have a wide range of applications in the pharmaceutical sector as anticancer, antimicrobial, insecticidal, and anti-parasitic agents [12]. Redstem filaree (*Erodium cicutarium*) is a spring flowering annual or biennial plant belonging to the Geraniaceae [13]. The antioxidant, antiviral, and spasmogenic activities of this plant's extract were reported [14]. *Erodium cicutarium* has been many pharmacological effects such as antioxidant, antiviral, antibacterial, and antifungal, interferon induction, anti-inflammatory, analgesic it is medicinal and therapeutic properties [15]. Devatha et al. [16] studied the effect of green synthesis of iron nanoparticles (done by *Azadirachta Indica* in different proportions) on antibacterial activity. Arokiyaraj et al. [17] investigated the enhanced antibacterial activity of iron oxide magnetic nanoparticles, treated with *Argemone Mexicana* L. leaf extract. Response surface methodology (RSM) is a mathematical technique applied in the progression of an appropriate functional relationship between the response and the related input variables. The main idea of RSM is to use a sequence of designed experiments to obtain an optimal response [18].

In the present study, plant extract of *E. cicutarium* was isolated using water bath method. The plant extract was then used for biosynthesis of Ag and Fe nanoparticles. Antibacterial activity was evaluated by MIC method. Optimal conditions were obtained by RSM based on CCD.

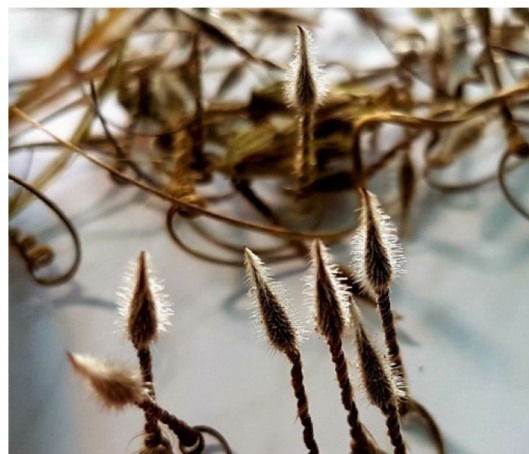


Fig. 1 *E. cicutarium* plant

Materials and methods

Materials

Fresh *E. cicutarium* plant (Fig. 1) was collected from its natural habitat, Hamadan Province, Iran. The samples were air-dried at room temperature. The dried samples were then grounded and stored at room temperature before analysis. All chemicals used in this study were of analytical grade and purchased from Merck (Darmstadt, Germany).

Preparation of extract plant

About 2 g grounded plant was mixed with 100 mL distilled water in an Erlenmeyer flask and heated at 80 °C for 30 min in a water bath. The solution was then filtered by Whatman filter paper and the extract was stored in the refrigerator at 4 °C for further studies.

Synthesis of Ag and Fe nanoparticles

An aliquot of 25.0 mL of the extract was mixed with 225 mL of 0.001 M AgNO_3 for Ag nanoparticle synthesis. The solution was shaken for 30 min and then stirred under sunlight for 10 min for the reaction to start.

Generally, a mixture of silver nitrate and plant extract in the case of a brightly colored production room brightens up from brown, but the addition of silver nitrate to the extract of *Erodium cicutarium* did not significantly change the color and the immediate change after the sunlight exposure was introduced. The presence of polyphenolic compounds, such as tannins, was affected by photo-oxidation. In the presence of sunlight; the ions of silver reduce to nanoparticle [19].



Table 1 Independent variables and their levels in the experimental

Ag and Fe nanoparticle		
Independent variables	Coded symbols	Levels
Concentration (µg/ml)	X_1	6, 63.70, 203, 342.30, 400
pH	X_2	4, 488, 7, 9.12, 10

The nanoparticle synthesis reaction was terminated by changing the color of the solution from yellow to brown–red. The solution containing the nanoparticles was then sealed in a flat-round bottle and stored in a dark place for 2 days for subsequent analyses. The synthesis reaction of the Fe nanoparticles was performed by mixing the extract with 0.1 M $\text{FeSO}_4 \cdot 7\text{H}_2\text{O}$ at a ratio of 1:2. The reaction was terminated when the color of the solution immediately changed from yellow to black. The solution contained significant amounts of the nanoparticles and then was stored at ambient temperature before analysis.

Design of the experiment

In this study, the main factor and their interactions were investigated. The effect of independent variables, including X_1 (concentration of nanoparticles) and X_2 (pH), were analyzed in five levels. These are shown in Table 1. The general equation of the response surface is defined as follows [18]:

$$Y = \beta_0 + \sum_{j=1}^k \beta_j X_j + \sum_{j=1}^k \beta_{jj} X_j^2 + \sum_i \sum_{<j=2}^k \beta_{ij} X_i X_j + e_i \quad (1)$$

where the predicted response is (predicted the diameter of the bacterial growth inhibition halo); X_i and X_j are the independent variables in coded levels; β_0 is the intercept and β_i , β_{jj} , β_{ij} are the linear squared and interaction effect coefficients, respectively; k is the number of factors (independent variables) and e_i is the model error.

Characterization of the Ag and Fe nanoparticles

UV–Vis spectroscopy analyses of the nanoparticles were carried out at ambient temperature, using a spectrophotometer (Varian, Cary 100 Cone model, USA). An aliquot of 200 µL of the solutions containing the Ag and Fe nanoparticles were diluted with 1000 mL of distilled water. The UV–Vis transmission spectra of the Ag and Fe nanoparticles were then obtained within the wavelength range of 380–550 nm and 200–600 nm, respectively.

FTIR transmission spectra of the samples were recorded by Thermo Nicolet spectrometer (Nexus 870, USA) with

a resolution of 4 cm^{-1} in the range $4000\text{--}500 \text{ cm}^{-1}$. The extract and the Ag and Fe nanoparticles were freeze dried. The samples were then pressed into KBr disks and their FTIR transmission spectra were obtained.

The morphology and sizes of the nanoparticles were analyzed by FE-SEM (Sigma, Oxford Instrument, UK). The following procedure was used to prepare the samples before FE-SEM analyses. A volume of the solutions containing the nanoparticles was poured into plastic vials and then the vials were centrifuged at 12,000 RPM for 5 min. The supernatant was discarded and distilled water was added to the wet precipitate for another centrifugal step. The vials were shaken vigorously and re-centrifuged at 12,000 rpm for another 5 min. The washing process of the precipitate was done thrice to obtain a precipitate with minimum impurity. Furthermore, ethanol was added to the wet precipitate and the vials were centrifuged under above-mentioned conditions. Finally, the supernatant was removed and the remaining wet precipitate was dried at 40°C in the oven, and used for FE-SEM and elemental composition analyses.

FE-SEM equipped with EXD detector was used for measuring the elemental composition of the nanoparticles.

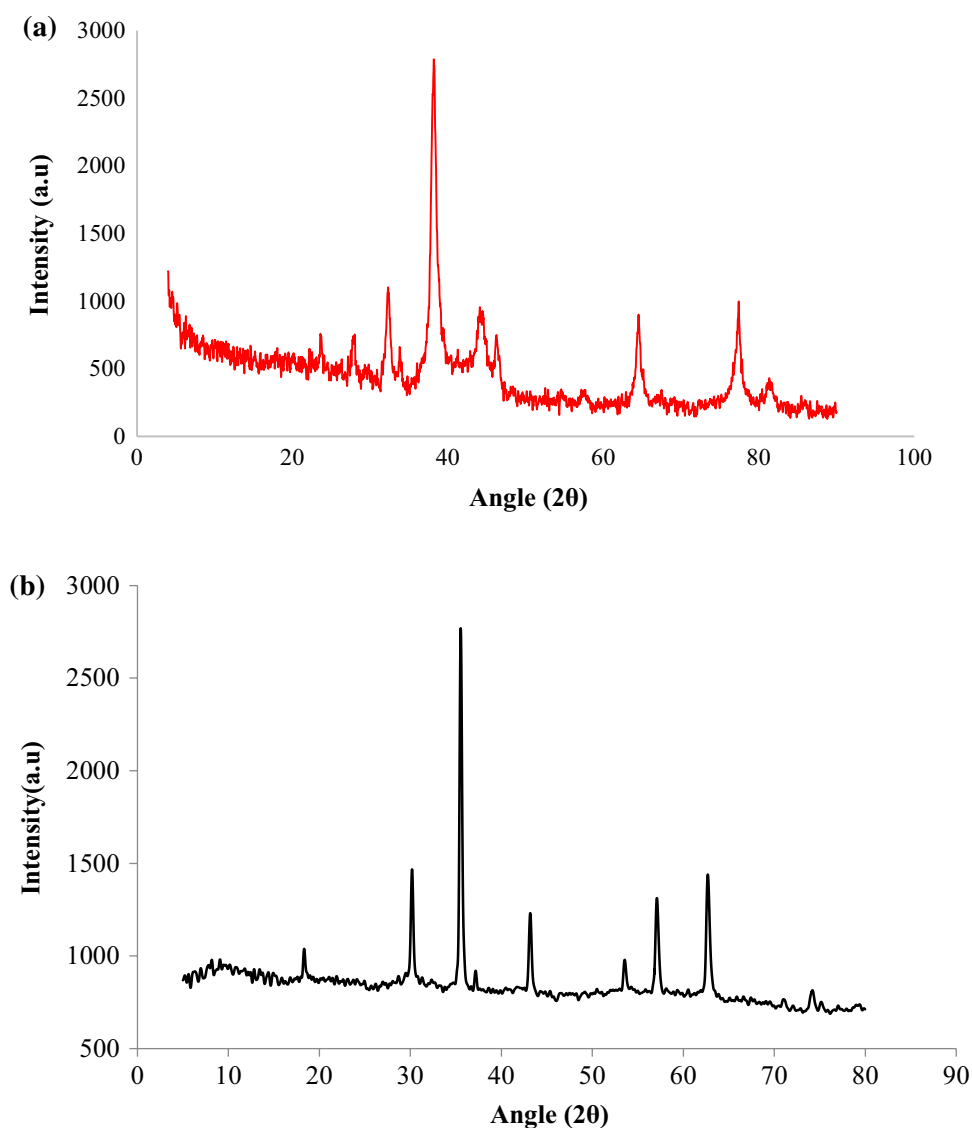
In vitro antibacterial activity of the Ag and Fe nanoparticles

The antimicrobial activity of the Ag and Fe nanoparticles were evaluated according to the MIC method. *Staphylococcus aureus* (ATCC 6538) *Escherichia coli* (ATCC 25922) were used in this study. To determine the antibacterial properties of Ag nanoparticles, the MIC method was used. The bacteria used in this study were prepared from the microbial bank of the Postor Institute of Iran. MIC testing was performed based on CLSI standard—by dilution method in microplate (CLSI 2012). The MIC concentration was determined for microorganism treated with different concentration of Ag and Fe nanoparticles. MIC refers to the lowest concentrations of compounds that inhibit the growth of microorganisms. Subsequently, 96 wells were prepared by distributing 195 µL of Muller Hinton Broth medium, containing each concentration of the nanoparticle with the desired pH and 5 µL of microbial inoculation into each of the wells. One well containing 195 µL of Muller Hinton Broth medium with 5 µL of microbial inoculation, as a positive control for each bacterium, and a well containing 195 µL of blank space was considered to be contralateral. The contents of each well—after mixing at 37°C for 24 h were incubated and the results were evaluated the next day.

As many as 13 experiments—with two factors, five levels, and two responses for *E.coli* (Gram-negative) and *S.aureus* (Gram-positive) bacteria—were designed by Design-Expert



Fig. 2 XRD spectra of **a** Ag and **b** Fe nanoparticles



software (Table 1). This was done to study the factors of concentration of Ag and Fe nanoparticles and pH and optimization of the process. In all the experiments, the diameter of the growth of halo of the bacteria is Response (R), the Gram-negative bacteria (R_1) and Gram-positive bacteria (R_2) were shown.

Results and discussion

Ag and Fe nanoparticles characterizations

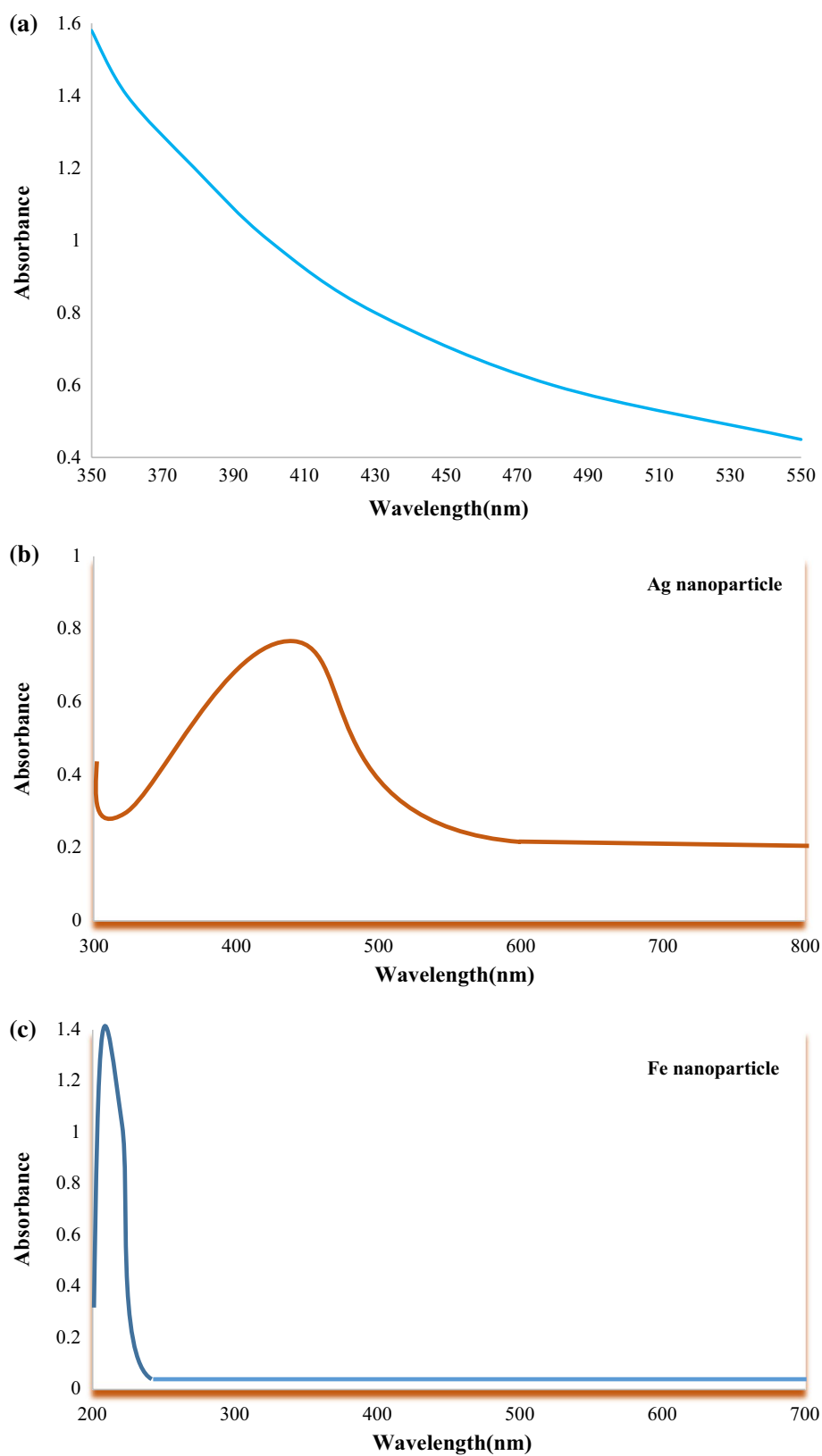
The XRD of Ag and Fe nanoparticles are shown in Fig. 2. As shown in Fig. 2a, Ag diffraction peaks at the angles of 38.11, 44.27, 64.42, 77.47 and 81.53° indicated (111), (200), (222),

(311), and (222), respectively, which confirmed the cubic phase and were directly matched with standard (JCPDS no. 00-004-0783). Also as shown in Fig. 2b, Fe_3O_4 diffraction peaks at the angles of 18.33, 30.15, 35.52, 43.17, 57.10 and 62.70° indicated (111), (220), (311), (400), (511), and (440), respectively, which confirmed the cubic phase and were directly matched with standard (JCPDS no. 01-088-0315).

The UV–visible spectra of the plant extract, Ag and Fe nanoparticles are shown in Fig. 3a–c, respectively. In Fig. 3a there is no indicator of peak. The peak at 420 nm was attributed to the surface plasmon resonance of Ag nanoparticles (Fig. 3b). Furthermore, the strongest absorbance peak at 230 nm was for the Fe nanoparticles (Fig. 3c). These absorption spectra indicated that the Fe and Ag nanoparticles were successfully synthesized.



Fig. 3 UV–visible spectra of **a** plant extract, **b** Ag and **c** Fe nanoparticles



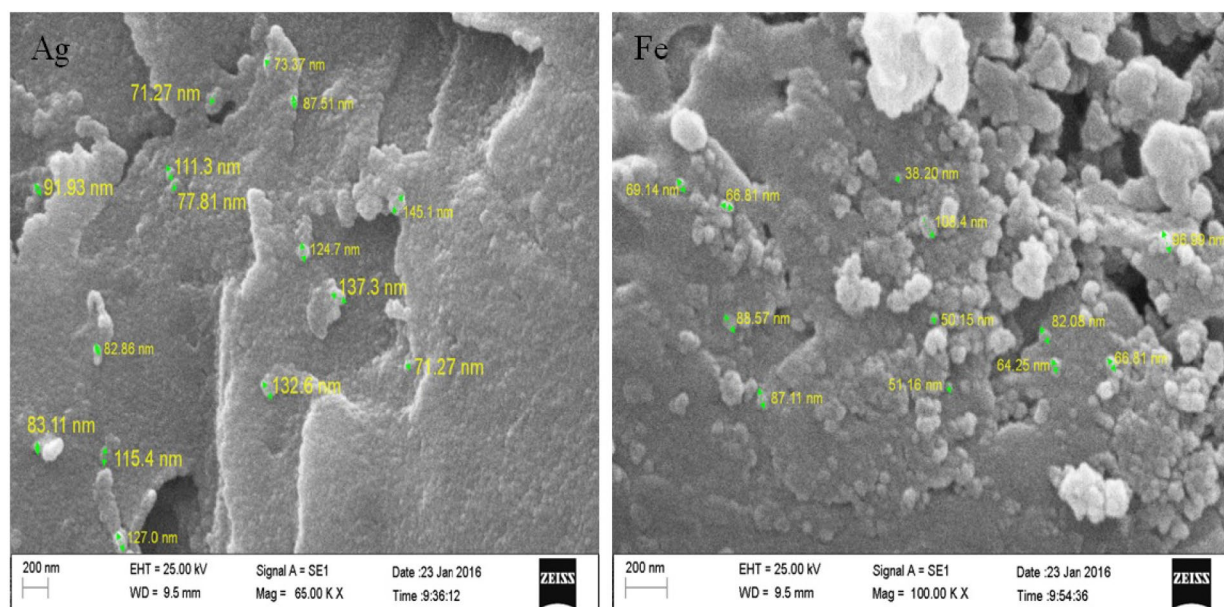


Fig. 4 FESEM images of Ag and Fe nanoparticles

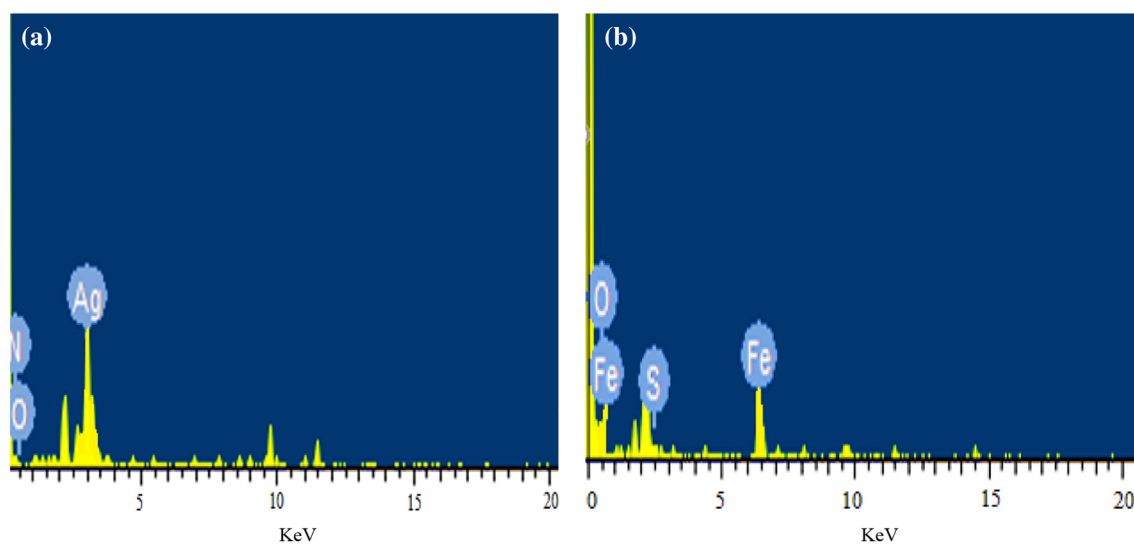


Fig. 5 EDX spectra of **a** Ag and **b** Fe nanoparticles

The size, shape, and morphologies of the formed Ag and Fe nanoparticles were characterized by FE-SEM. According to the FE-SEM images of the Ag and Fe particles (Fig. 3), these nanoparticles had nearly spherical morphology. Furthermore, the average particle size of the formed nanoparticles was estimated from the FE-SEM images. According to the results, most of the nanoparticles had average diameter of less than 100 nm. This indicated that more uniform and

nano-dimensional particles were formed by the extraction method. The Ag nanoparticles with size distribution of 55–80 nm and average diameter of about 64.8 nm were bio-synthesized using novel sundried *Cinnamomum camphora* leaf by [20].

According to the analysis of EDX spectrometers (Fig. 4), the presence of the elemental Ag and Fe signals, corresponding to the Ag and Fe nanoparticles, was confirmed.



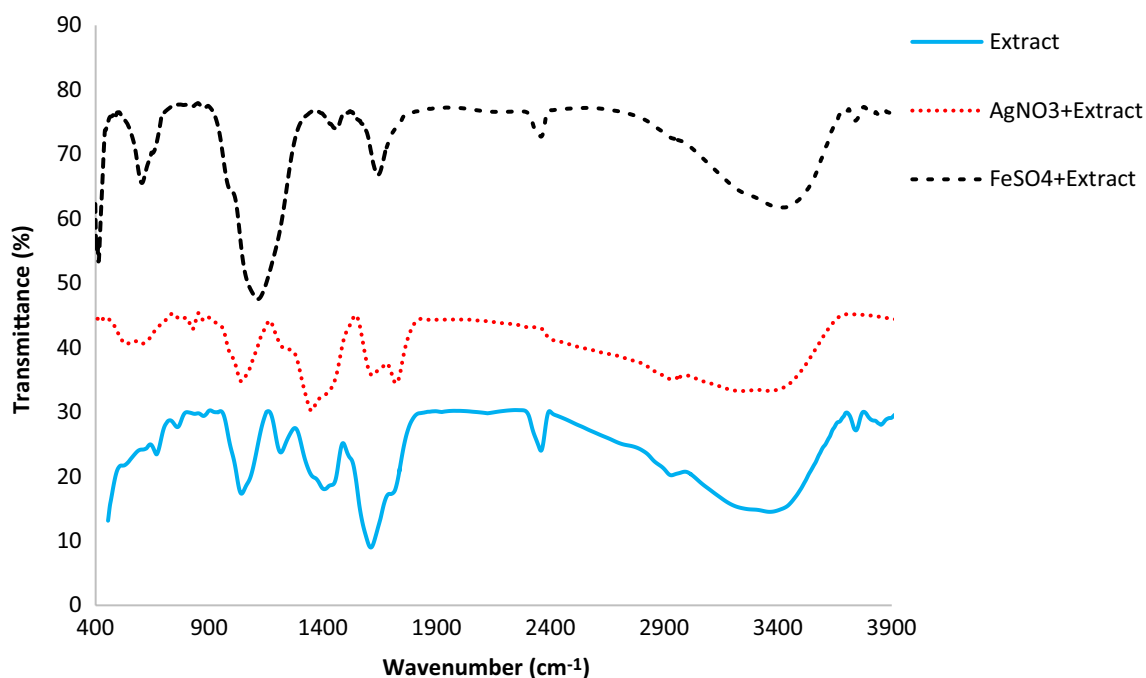


Fig. 6 FTIR spectra of the extract and the Ag and Fe nanoparticles

Furthermore, Ag and Fe were correctly identified by displacing the identification lines for the major emission energies for Ag and Fe. In general, it was seen from the EDX spectrometers that the impurity and presence of different chemicals, in the form nanoparticles, were relatively low. Moreover, the structures of the nanoparticles were rich in Ag and Fe elements.

The FTIR spectra of the *E. cicutarium* extract and the Ag and Fe nanoparticles are shown in Fig. 5. The sharp band centered at about 700 cm^{-1} is likely due to the bending modes of groups such as $=\text{CH}$, $=\text{CH}_2$, and *cis*- $\text{CH}=\text{CH}$ (alkenes); CH_3 , CH_2 , and CH (alkanes); NH_2 (amines); and the bonds of $\text{C}-\text{H}$ (aromatic rings) and $\text{O}-\text{H}$ (alcohols and phenols). In addition, a relatively sharp band centered at around 1600 cm^{-1} could be due to the bending modes of the $\text{N}-\text{H}$ and $\text{C}=\text{O}$ bonds of carboxylic acids and derivatives, NH_2 groups of amines as well as the stretching modes of $\text{C}=\text{C}$ bonds of aromatic rings and alkenes. Furthermore, the bending modes of the $\text{N}-\text{H}$ bonds (carboxylic acids and derivatives) and the scissoring mode of the NH_2 groups (amines) could be seen at wave number displaced between 1650 and 1665 cm^{-1} [11].

The bands appearing at 2880 – 2990 cm^{-1} are attributed to the stretching modes of the groups of CH_3 , CH_2 , and CH in alkanes and also to the stretching vibration of the $\text{O}-\text{H}$ bonds of carboxylic acids and derivatives. The bands at 1440 and 1222 cm^{-1} could be due to the $\text{C}-\text{O}-\text{H}$ vibrations

and polyphenols, respectively. These bands also appear on the spectra of the extract and the Ag nanoparticles, but are weak on the Fe nanoparticle spectrum. In general, the strong intense bands appear at 3400 , 1600 , and 1100 cm^{-1} are due to the H bonds, amide groups, $\text{C}-\text{O}$ bonds, and stretching modes. This indicates the presence of active groups ($-\text{COOH}$) responsible for synthesizing of the nanoparticles. These results indicate that *E. cicutarium* extract acts as a reducing and stabilizing agent for Ag and Fe particles. Based on the results the *E. cicutarium* extract contained alkaloids, proteins, enzymes, amino acids, alcoholic compounds, and polysaccharides, which were said to be responsible for the reduction of the Ag and Fe ions to nanoparticles [21, 22].

One of the methods of nanoparticle analysis is the dynamic light scattering analyses (DLS), which has the ability to quickly and simply measure particles inside the solution. In this study, DLS analysis was used to determine the size of Ag and Fe nanoparticles. Figure 6a, b shows the results of Ag and Fe nanoparticles, respectively. Based on the results, the average particle size of Ag and Fe nanoparticles are 21.4 and 32.2 nm , respectively.

Modeling and analysis of variance (ANOVA)

According to the designed experiments, 13 experiments were carried out to evaluate the antibacterial activity of Ag and Fe nanoparticles in vitro. Table 2 shows the results



Table 2 The central composite design for the two independent variables

RUN no.	Concentration ($\mu\text{g/ml}$)	PH	Ag nanoparticle		Fe nanoparticle	
			R_1	R_2	R_1	R_2
1	400	7	24	21	22	18
2	63.70	4.88	3	5	3	4
3	203	7	4	5	5	7
4	6	7	7	5	4	6
5	203	7	5	7	5	7
6	203	10	20	19	17	6
7	203	7	4	5	5	7
8	342.30	4.88	20	18	15	16
9	203	4	6	4	6	8
10	203	7	4	5	5	6
11	203	7	4	5	5	7
12	63.70	9.12	5	4	4	6
13	342.30	9.12	16	21	21	17

Table 3 ANOVA for analysis of variance and adequacy of the quadratic model for Ag nanoparticles

Source	Ag nanoparticle (R_1)				Ag nanoparticle (R_2)					
	Sum of squares	Degree of freedom	Mean square	F value	P value Prob > F	Sum of squares	Degree of freedom	Mean square	F value	p value Prob > F
Model	611.79	5	122.6	10.28	0.0040	504.17	5	100.83	17.39	0.0008
Concentration ($\mu\text{g/ml}$)	338.54	1	338.54	28.45	0.0011	271.76	1	271.76	46.86	0.0002
pH	39.60	1	39.60	3.33	0.1109	79.46	1	79.46	13.70	0.0076
AB	9.00	1	9.00	0.76	0.4131	1.00	1	1.00	0.17	0.6904
A^2	162.79	1	162.79	13.68	0.0077	103.78	1	103.78	17.89	0.0039
B^2	89.53	1	89.53	7.53	0.0288	67.39	1	67.39	11.62	0.0113
Residual	83.28	7	11.90			40.60	7	5.80		
Lack of fit	82.48	3	27.49	137.47	0.0002	37.40	3	12.47	15.58	0.0113
Pure Error	0.80	4	0.20			3.20	4	0.80		



Table 4 ANOVA for analysis of variance and adequacy of the quadratic model for Fe nanoparticles

Source	Fe nanoparticle (R_1)					Fe nanoparticle (R_2)				
	Sum of squares	Degree of freedom	Mean square	F value	p value Prob > F	Sum of squares	Degree of freedom	Mean square	F value	p value Prob > F
Model	572.78	5	114.56	52.68	<0.0001	258.98	5	51.80	28.51	0.0002
Concentration ($\mu\text{g/ml}$)	370.68	1	370.68	170.47	<0.0001	199.71	1	199.71	109.94	<0.0001
pH	63.60	1	63.60		0.0010	3.680e-003	1	3.680e-003	2.026e-003	0.9654
AB	6.25	1	6.25	29.25	0.1338	0.25	1	0.25	0.14	0.7216
A ²	91.41	1	91.41	2.87	0.0003	59.01	1	59.01	32.49	0.0007
B ²	57.50	1	57.50	42.04	0.0013	1.18	1	1.18	0.65	0.4461
Residual	15.22	7	2.17	26.44		12.72	7	3.97		
Lack of fit	15.22	3	5.07		0.0001	11.92	3	0.20	19.86	0.0073
Pure error	0.0001	4	0.0001	14.39		0.80	4			

Table 5 Correlation coefficients (R^2) and adjusted coefficients (R^2 adjusted) For Ag and Fe nanoparticles

	Ag nanoparticle		Fe nanoparticle	
	R_1	R_2	R_1	R_2
R^2	0.8802	0.9225	0.9741	0.9532
R^2 predicted	0.7946	0.8722	0.9558	0.9198

of the experiments. Using regression coefficients, the antibacterial property effect of Ag and Fe nanoparticles on the dependent variables was calculated. Tables 3 and 4 show the results of the statistical analysis. For the model to have a good ability to fit the information, it was necessary that the correlation coefficients (R^2) and adjusted coefficients (R^2 adjusted) to have the highest value. In this study, R^2 and R^2 adjusted for Ag and Fe nanoparticles, are shown in Table 5. The results showed that the models were of high significance. The assumption of normal data is shown in Figs. 7 and 8. The data were almost normal and graph showed the normal probability of how the residues followed a normal distribution. Linear equations in coded form are shown below:

$$R_1(\text{mm}) = + 4.20 + 6.51 - A + 2.22 - B + 1.50 - A - B + 4.84 - A^2 + 3.59B^2 \quad (2)$$

$$R_2(\text{mm}) = + 5.40 + 5.83 - A + 3.15 - B - 0.50 - A - B + 3.86 - A^2 + 3.11B^2 \quad (3)$$

Fe nanoparticles:

$$R_1(\text{mm}) = + 5.00 + 6.81 - A + 2.82 - B + 1.25 - A - B + 3.62 - A^2 + 2.88B^2 \quad (4)$$

$$R_2(\text{mm}) = + 6.80 + 5.00 - A + 0.021 - B - 0.25 - A - B + 2.91 - A^2 + 0.41B^2 \quad (5)$$

Investigation of the concentration Ag and Fe nanoparticles and pH parameters in antibacterial activity

Figures 9 and 10 show the effect of the concentration of Ag and Fe nanoparticles, pH, and the interaction between them in the diameter of the bacterial growth inhibition halo in the form of contour plot and three-dimensional, respectively. As can be seen, the pH diameter of the bacterial growth inhibition halo increased with an increase in the concentration of Ag and Fe nanoparticles. The results showed that the concentration of Ag and Fe nanoparticles had a better effect on antibacterial activity. By increasing the concentration of Ag nanoparticles from 6 to 400,



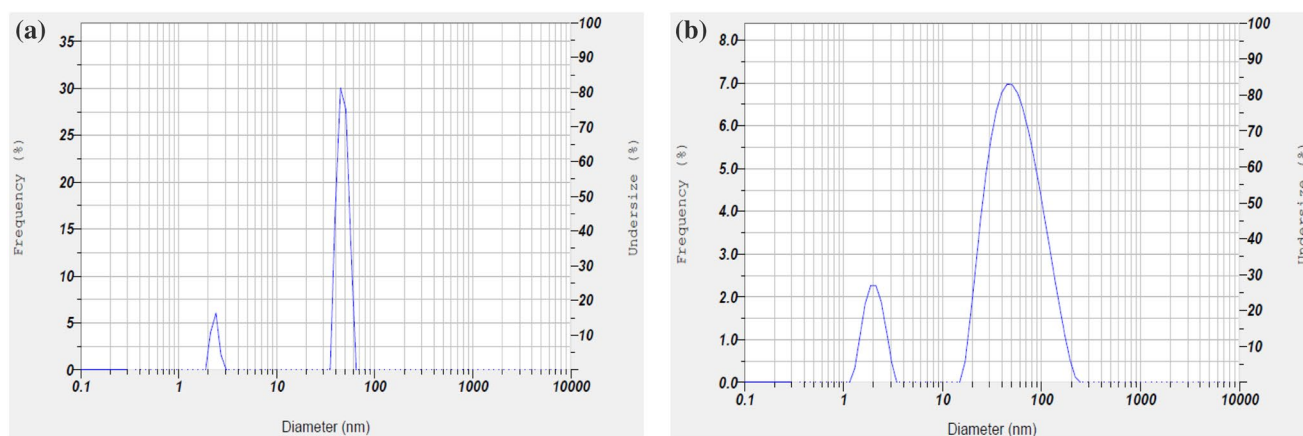


Fig. 7 DLS analyses **a** Ag and **b** Fe nanoparticles

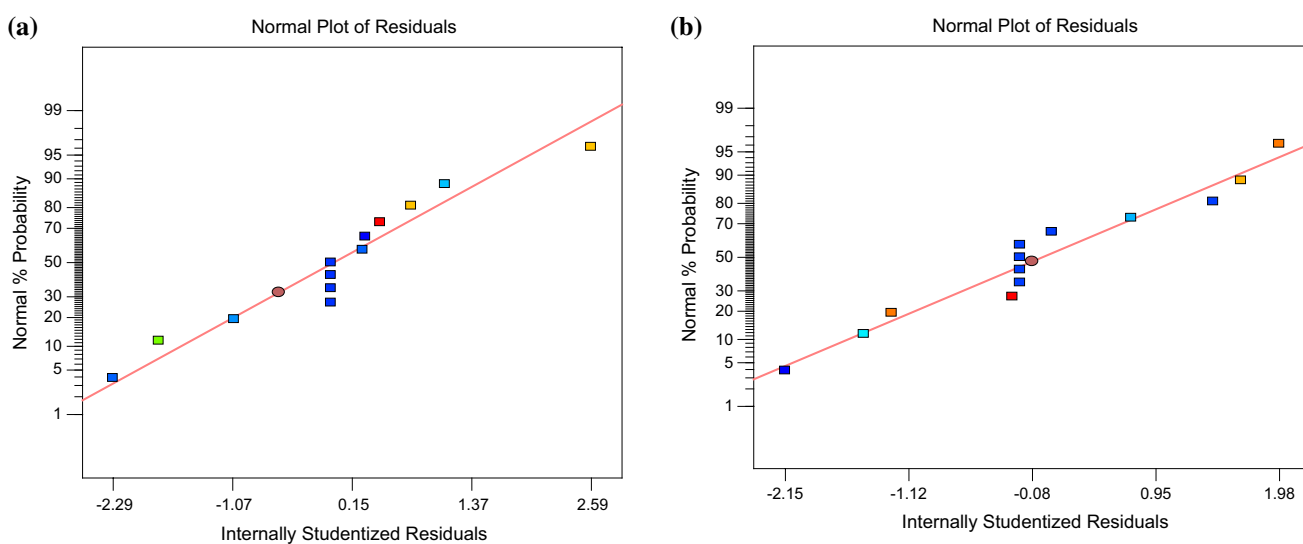


Fig. 8 Normal probability plot of the studentized residual for: diameter of the bacterial growth inhibition halo by Ag nanoparticles **a** R_1 , **b** R_2

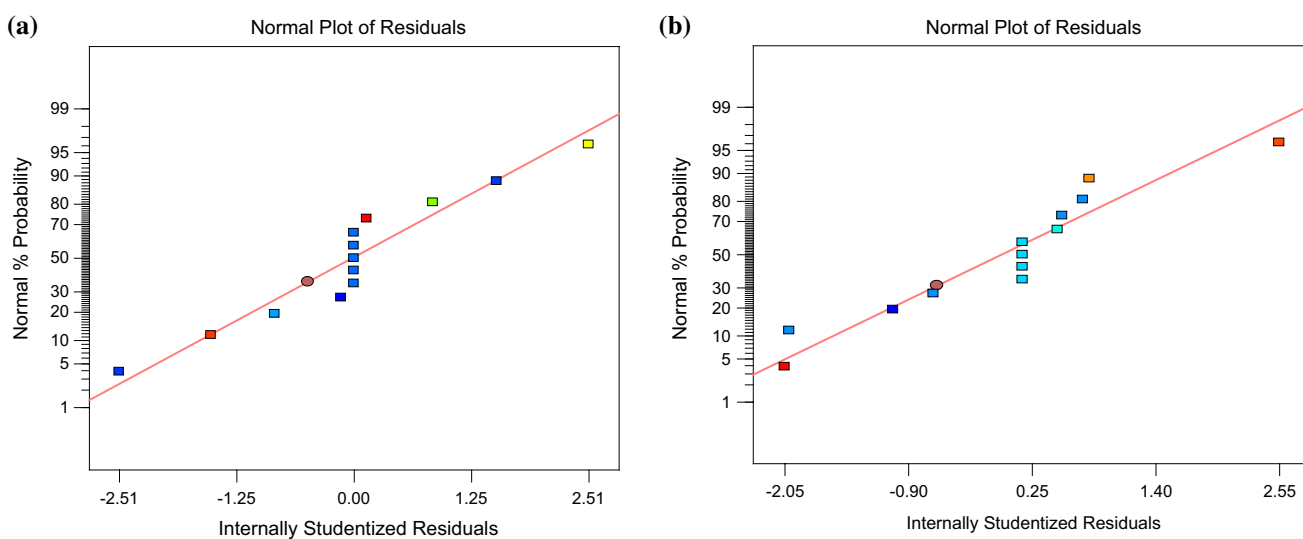


Fig. 9 Normal probability plot of the studentized residual for: diameter of the bacterial growth inhibition halo by Fe nanoparticles **a** R_1 , **b** R_2



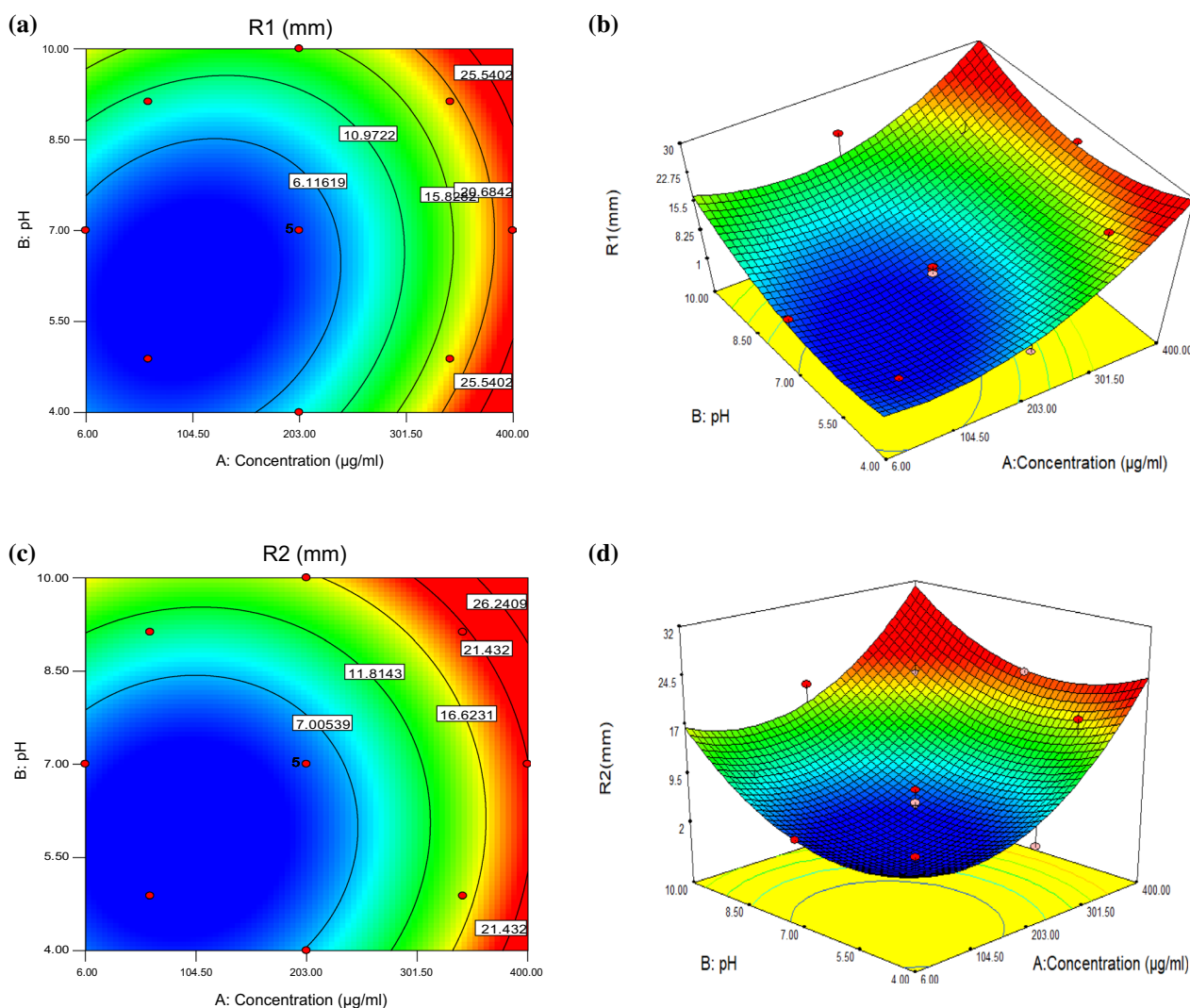


Fig. 10 Function of concentration and pH in diameter of the bacterial growth inhibition halo by Ag nanoparticles **a** Contour plot (R_1), **b** 3D surface (R_1), **c** Contour plot (R_2), **d** 3D surface (R_2)

the diameter of the growth inhibition R_1 increased from 7 to 24 and R_2 increased from 5 to 21 increased. The result showed that by increasing pH from 4 to 10, the diameter of the growth inhibition R_1 increased from 6 to 20 and R_2 increased from 4 to 19 (Fig. 8). Moreover, by increasing the concentration of Fe nanoparticles from 6 to 400 (μg/mL), the diameter of the growth inhibition R_1 increased from 4 to 22 and R_2 increased from 6 to 18. The result showed that by increasing the pH value from 4 to 10, the diameter of the growth inhibition R_1 and R_2 increased from 6 to 17 and from 8 to 16, respectively

(Fig. 10). Furthermore, the results showed that the Ag and Fe nanoparticles had greater effect on the *E. coli* bacterium, where the Ag nanoparticles performed better than the Fe nanoparticles.

Optimization of pH and concentration of Ag and Fe nanoparticles

Experimental design studies optimal point conditions was obtained. Under optimal conditions, with a concentration of Ag and Fe nanoparticles at 399.53 and 397.38 (μg/mL) and



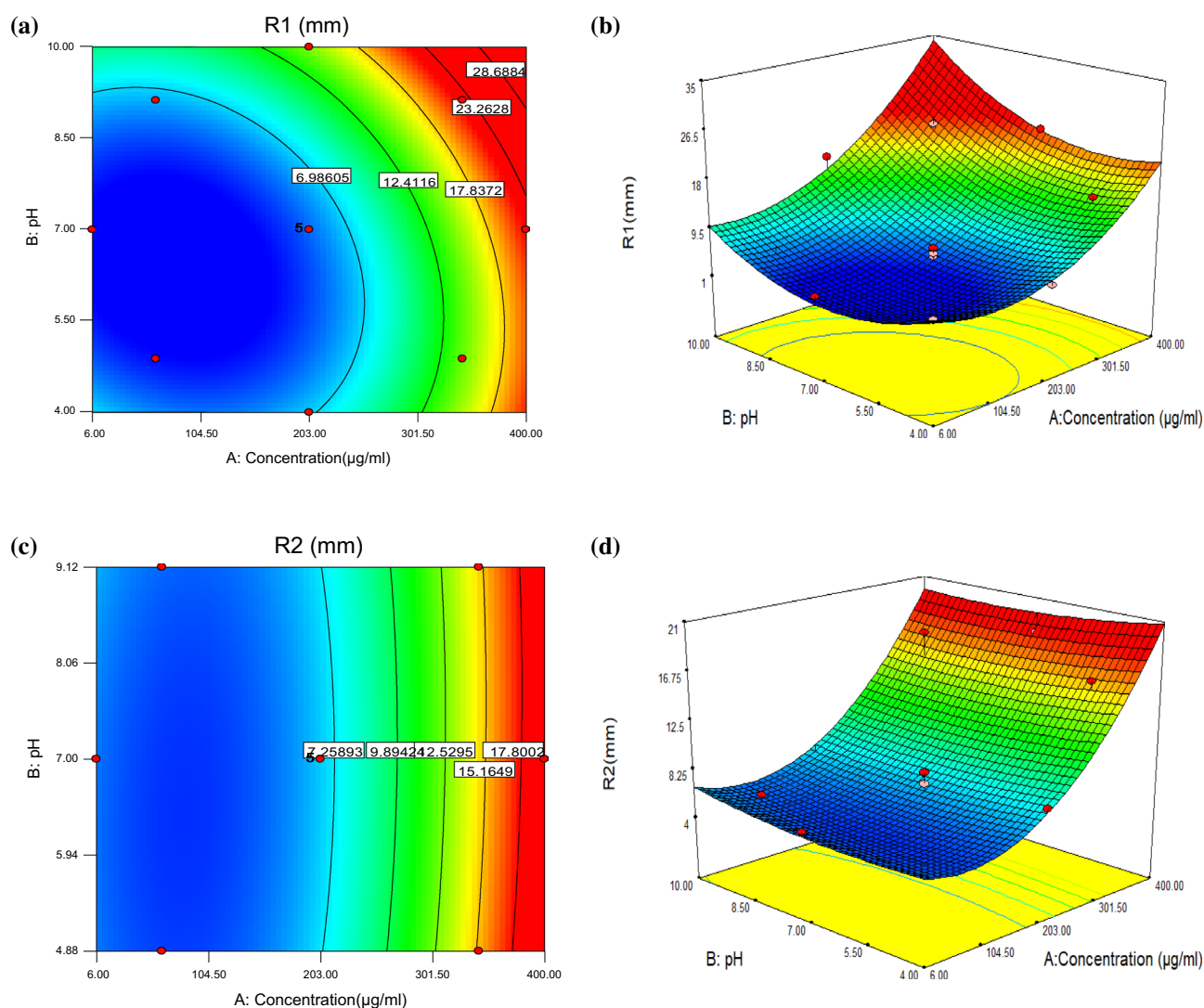


Fig. 11 Function of concentration and pH in diameter of the bacterial growth inhibition halo by Fe nanoparticles **a** Contour plot (R_1), **b** 3D surface (R_1), **c** Contour plot (R_2), **d** 3D surface (R_2)

pH values of 8.20 and 8.39 was found to have the highest amount of growth inhibitory halo diameter (Fig. 11).

A simple and efficient way to synthesize the Ag and Fe nanoparticles by *E. cicutarium* was reported in this study. The optimization and the modeling [18] of diameter of the bacterial growth inhibition halo were performed using a composite experimental design. Under optimal conditions, with a concentration of Ag and Fe nanoparticles at 399.53

and 397.38 (μg/mL), pH values of 8.20 and 8.39 were found to have the highest amount of growth inhibitory halo diameter. The results showed that the Ag and Fe nanoparticles had a greater effect on the *E. coli* cumins, where Ag nanoparticles had a better performance than the Fe nanoparticles (Fig. 12).



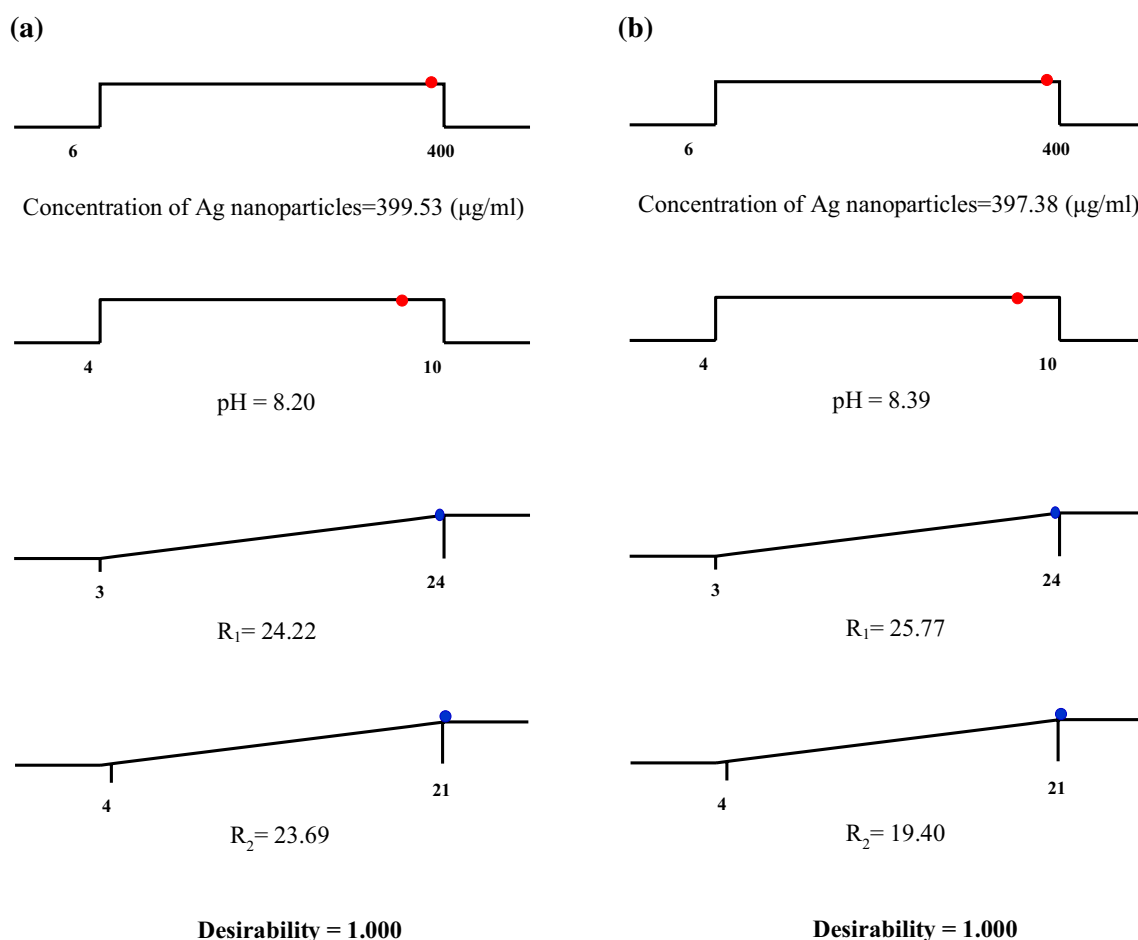


Fig. 12 Graphs the optimum conditions of diameter of the bacterial growth inhibition halo by **a** Ag nanoparticles, **b** Fe nanoparticles

Open Access This article is distributed under the terms of the Creative Commons Attribution 4.0 International License (<http://creativecommons.org/licenses/by/4.0/>), which permits unrestricted use, distribution, and reproduction in any medium, provided you give appropriate credit to the original author(s) and the source, provide a link to the Creative Commons license, and indicate if changes were made.

References

- Vidhu, V.K., Aromal, S.A., Philip, D.: Green synthesis of silver nanoparticles using *Macrotyloma uniflorum*. Spectrochim. Acta Part A **83**(1), 392–397 (2011)
- Logeswari, P., Silambarasan, S., Abraham, J.: Ecofriendly synthesis of silver nanoparticles from commercially available plant powders and their antibacterial properties. Sci. Iran. **20**(3), 1049–1054 (2013)
- Sholkamy, E.N., Ahamd, M.S., Yasser, M.M., Eslam, N.: Antimicrobial activities of bio-synthesized silver nano-stars by *Saccharopolyspora hirsute*. Saudi J. Biol. Sci. **26**(1), 195–200 (2019)
- Li, J., Tian, B., Li, T., Dai, S.H., Weng, Y., Lu, J., Xu, X., Jin, Y., Pang, R., Hua, Y.: Biosynthesis of Au, Ag and Au–Ag bimetallic nanoparticles using protein extracts of *Deinococcus radiodurans* and evaluation of their cytotoxicity. Int. J. Nanomed. **13**, 1411–1424 (2018)
- Azlin-Hasim, S., Cruz-Romero, M.C., Ghoshal, T., Morris, M.A., Cummins, E., Kerry, J.P.: Application of silver nanodots for potential use in antimicrobial packaging applications. Innov. Food Sci. Emerg. Technol. **27**, 136–143 (2015)
- Gardea-Torresdey, J.L., Gomez, E., Peralta-Videa, J.R., Parsons, J.G., Troiani, H., Jose-Yacamán, M.: Alfalfa sprouts: a natural source for the synthesis of silver nanoparticles. Langmuir **19**(4), 1357–1361 (2003)
- Gardea-Torresdey, J.L., Parsons, J.G., Gomez, E., Peralta-Videa, J., Troiani, H.E., Santiago, P., Yacamán, M.J.: Formation and growth of Au nanoparticles inside live alfalfa plants. Nano Lett. **2**(4), 397–401 (2002)
- Chandran, S.P., Chaudhary, M., Pasricha, R., Ahmad, A., Sastry, M.: Synthesis of gold nanotriangles and silver nanoparticles using *Aloe vera* plant extract. Biotechnol. Prog. **22**(2), 577–583 (2006)
- Huang, J., Li, Q., Sun, D., Lu, Y., Su, Y., Yang, X., Wang, Y., Shao, W., He, N., Hong, J.: Biosynthesis of silver and gold nanoparticles by novel sundried *Cinnamomum camphora* leaf. Nanotechnology **18**(10), 105104 (2007)
- Roopan, S.M., Madhumitha, G., Rahuman, A.A., Kamaraj, C., Surendra, A., Bharathi, T.V.: Low-cost and eco-friendly phyto-synthesis of silver nanoparticles using *Cocos nucifera* coir extract and its larvicidal activity. Ind. Crops Prod. **43**, 631–635 (2013)



11. Ulug, B., Turkdemir, M.H., Cicek, A., Mete, A.: Role of irradiation in the green synthesis of silver nanoparticles mediated by fig (*Ficus carica*) leaf extract. *Spectrochim. Acta Part A* **135**, 153–161 (2015)
12. Qi, X.L., Li, T.T., Wei, Z.F., Guo, N., Luo, M., Wang, W., Zu, Y.G., Fu, Y.J.: Peng X (2014) Solvent-free microwave extraction of essential oil from pigeon pea leaves [*Cajanus cajan* (L.) Millsp.] and evaluation of its antimicrobial activity. *Ind. Crops Prod.* **58**, 322–328 (2014)
13. Odero, D.C., Mesbah, A.O., Miller, S.D., Kniss, A.R.: Interference of redstem filaree (*Erodium cicutarium*) in sugar beet. *Weed Sci.* **59**(3), 310–313 (2011)
14. Tian, Y., Puganen, A., Alakomi, H.L., Uusitupa, A., Saarela, M., Yang, B.: Antioxidative and antibacterial activities of aqueous ethanol extracts of berries, leaves, and branches of berry plants. *Food Res. Int.* **106**, 291–303 (2018)
15. Al-Snafi, A.S.: A review on *Erodium Cicutarium*: a potential medicinal plant. *IAJPS* **4**(01), 110–116 (2017)
16. Devatha, C.P., Jagadeesh, K., Patil, M.: Effect of green synthesized iron nanoparticles by *Azadirachta Indica* in different proportions on antibacterial activity. *Environ. Nanotechnol. Monit. Manag.* **9**, 85–94 (2018)
17. Arokiyaraj, S., Saravanan, M., Prakash, N.K.U., Valan, A.M., Vijayakumar, B.: Vincent S (2013) Enhanced antibacterial activity of iron oxide magnetic nanoparticles treated with *Argemone mexicana* L. leaf extract: an in vitro study. *Mater. Res. Bull.* **48**(9), 3323–3327 (2013)
18. Kashi, N., Elmi Fard, N., Fazaeli, R.: Empirical modeling and CCD-based RSM optimization of Cd(II) adsorption from aqueous solution on clinoptilolite and bentonite. *Russ. J. Appl. Chem.* **90**(6), 977–992 (2017)
19. Vinod Kumar, V., Anbarasan, S., Christena, L.R., SaiSubramanian, N., Philip Anthony, S.: Bio-functionalized silver nanoparticles for selective colorimetric sensing of toxic metal ions and antimicrobial studies. *Spectrochim. Acta A Mol. Biomol. Spectrosc.* **129**, 35–42 (2014)
20. Huang, D., Ou, B., Prior, R.L.: The chemistry behind antioxidant capacity assays. *J. Agric. Food Chem.* **53**(6), 1841–1856 (2005)
21. Anandalakshmi, K., Venugobal, J., Ramasamy, V.: Characterization of silver nanoparticles by green synthesis method using *Petalium murex* leaf extract and their antibacterial activity. *Appl. Nano Sci* **6**, 399–408 (2016)
22. Wang, T., Jin, X., Chen, Z., Megharaj, M., Naidu, R.: Green synthesis of Fe nanoparticles using eucalyptus leaf extracts for treatment of eutrophic wastewater. *Sci. Total Environ.* **466–467**, 210–213 (2014)

Publisher's Note Springer Nature remains neutral with regard to jurisdictional claims in published maps and institutional affiliations.

Affiliations

Nahid Maghsoudy¹ · Parviz Aberoomand Azar¹ · Mohammad Saber Tehrani¹ · Syed Waqif Husain¹ · Kambiz Larijani¹

Nahid Maghsoudy
nahidmaghsoudy@gmail.com

Mohammad Saber Tehrani
drmsabertehrani@yahoo.com

Syed Waqif Husain
V-hosein@srbiau.ac.ir

Kambiz Larijani
Larijani_k@yahoo.com

¹ Department of Chemistry, Science and Research Branch, Islamic Azad University, Tehran, Iran

